Limit equilibrium slope stability analysis using rigid finite elements

Dieter Stolle and Peijun Guo

Abstract: This paper revisits the interslice force assumptions associated with the method-of-slices approach to slope stability analysis. A brief review is presented on analysis procedures for this class of problem and a comparison is made between the factor of safety equations derived by Fellenius and a modified form of Bishop's equation. A simplified rigid finite element method that takes into account progressive yielding through a sliding law is proposed, eliminating the need to provide constraint equations for the variation of interslice forces required by more advanced procedures, such as that developed by Morgenstern and Price. An example is given to demonstrate the proposed procedure and to investigate the sensitivity of the global and local factors of safety to the interslice and basal shear forces. It is demonstrated that the global factor of safety tends not to be sensitive to interslice shear forces when dealing with circular slip. For the slip circles that were analyzed, the Morgenstern and Price procedure yielded slice forces that were similar to those predicted by the proposed method, which takes into account the deformation and failure characteristics of the material comprising the slope.

Key words: slope stability, rigid finite elements, limit equilibrium.

Résumé : Cet article revoit les hypothèses de forces entre les tranches associées à la méthode de l'approche des tranches dans l'analyse de stabilité des talus. On présente une brève revue des procédures d'analyse pour cette classe de problème et on fait une comparaison entre les équations du coefficient de sécurité de Fellenius et une forme modifiée de l'équation de Bishop. On propose alors une méthode d'éléments finis rigides simplifiée qui prend en compte une déformation progressive dans une loi de glissement, éliminant le besoin de fournir des équations contraignantes pour la variation des forces entre les tranches requises par les procédures plus élaborées telles que celle de Morgenstern et Price. On donne un exemple pour démontrer la procédure proposée et pour étudier la sensibilité des coefficients de sécurité local et global à l'intertranche et aux forces de cisaillement à la base. On démontre que le coefficient de sécurité global tend à ne pas être sensible aux forces de cisaillement intertranche lorsque l'on traite d'un glissement circulaire. Pour les glissements circulaires qui ont été analysés, la procédure de Morgenstern et Price a donné des forces entre les tranches qui étaient similaires à celles prédites par la méthode proposée qui prend en compte la déformation et les caractéristiques de rupture du matériau constituant le talus.

Mots-clés : stabilité de talus, éléments finis rigides, équilibre limite.

[Traduit par la Rédaction]

Introduction

From design and analyses points of view, geotechnical engineers are interested in the stability and serviceability of geotechnical structures, including bearing capacity, lateral earth pressures, and slope stability. Historically, these considerations have been uncoupled, with stability analyses not taking into account deformation history but rather focusing on limiting states and mechanisms leading to failure. Although modern computer analyses tools can easily accommodate the coupling between deformation history and failure, the input required for detailed analyses is often missing, leaving the engineer to rely on traditional approaches that require less data input.

An objective of this paper is to present a rigorous but simplified methodology that combines the finite element and limit equilibrium procedures for analyzing slope stability of natural and manmade slopes. A second objective is to examine interslice forces that develop when taking into account the kinematics and to compare the solutions with those obtained by more traditional methods, which neglect the coupling between forces and kinematics.

We begin with a brief literature review and discussion on the uniqueness of failure mechanisms. Thereafter, the factor of safety equations derived by Fellenius and a modified form of Bishop's method are presented to highlight the importance of modeling assumptions. A method-of-slices approach is then presented followed by an example that investigates the significance of interslice forces on computed factors of safety. The proposed method-of-slices procedure enforces force equilibrium on the local and global levels and calculates the corresponding global factor of safety

Received 9 June 2007. Accepted 9 January 2008. Published on the NRC Research Press Web site at cgj.nrc.ca on 20 May 2008.

D. Stolle[1] and P. Guo. Centre of Effective Design of Structures, Department of Civil Engineering, McMaster University, Hamilton, ON L8S 4L7, Canada.

[1]Corresponding author (e-mail: stolle@mcmaster.ca).

 doi:10.1139/T08-010

based on moment equilibrium. It accommodates progressive failure by taking into account a constitutive relation between the stresses and the relative movement between slices.

Background

Various procedures are available for the stability analysis, including: limit equilibrium analysis, application of limit theorems of plasticity, and the use of the finite element method (FEM). A brief review of these procedures follows.

Limit equilibrium

Of the various analysis frameworks, limit equilibrium methods are most often used when studying slope stability. A slope is usually assumed to fail along a distinct failure surface that could be of circular or noncircular form. When dealing with nonhomogeneous and irregular slopes, the method-of-slices is most often adopted, wherein a potential failure surface is defined and the slope is subdivided into slices. Figure 1 shows an assumed circular arc failure surface, as well as a free body diagram of a slice containing the internal and external forces. Strictly speaking, one must consider force $\Sigma \vec{F} = 0$ and moment $\Sigma \vec{r} \times \vec{F} = 0$ equilibrium on both the local and global levels when analyzing the stability of a slope. The problem that arises is that one has more unknowns than equations, and therefore assumptions must be made regarding the interslice forces if the deformation and stress–strain characteristics are not taken into account. Fredlund and Krahn (1977) compare several methods-of-slices and show that the manner in which interslice forces are handled has an impact on the global factor of safety.

Research into the development of the method-of-slices has been along two fronts: the development of algorithms for identifying the critical failure surface corresponding to the minimum factor of safety (Baker 1980; Li and White 1987; De Natale 1991; Malkawi et al. 2001; Zhu et al. 2005; Zolfaghari et al. 2005); and refining the simplifications with regards to satisfying equilibrium conditions on the local and global levels; see, for example, Bishop (1955); Morgenstern and Price (1965); Spencer (1967). A difficulty that arises is the presence of multiple local minima points; see, for example, Chen and Morgenstern (1983); and Chen and Shao (1988). There is no guarantee that the failure surface that has been identified corresponds to the global minimum factor of safety.

A review of the literature indicates that the Morgenstern and Price (M–P) procedure appears to be the most popular with regard to those methods that can accommodate general failure surfaces. The reader is referred to Duncan and Wright (2005) for a review of the various procedures, including assumptions, equilibrium conditions, and unknowns that are being solved for.

Finite element analysis

Finite element modeling has the advantage over classical limit equilibrium methods as no presumed failure surface or failure mechanism is required because failure occurs "naturally" taking into account the nonlinear relation between stresses and strains. The procedure allows a detailed description of the soil profile and preserves global equilibrium until "failure" occurs. Introduction of constitutive laws that accommodate failure avoids the need to make the limit equilibrium assumption that shear strength is mobilized uniformly along a well-defined sliding surface that must be identified as part of the solution process. As a result, the predictions are believed to be more representative of what is actually taking place within and around a slope; see, for example, Lane and Griffiths (1997). Pham and Fredlund (2003) developed a strategy making use of finite element solutions and dynamic programming, which was later modified by Stolle et al. (2004) to accommodate more general yield functions, to determine the critical slip surfaces.

Limit analysis

In spite of the popularity of limit equilibrium strategies, both kinematic and static admissibility are violated potentially leading to significant errors in factor of safety estimates (Yu et al. 1998). A more rigorous approach makes use of the limit theorems of plasticity to provide lower (Sloan 1988) and upper (Sloan 1989) bound solutions based on equilibrium and collapse mechanisms, respectively; also see, for example, Kim et al. (2002). A compromise between limit equilibrium and limit analysis, referred to as the kinematic element method (KEM), was developed by Gussmann (2000). In this method both the kinemetics and static equilibrium of rigid elements are rigorously taken into account to determine limit–load solutions or factors of safety. Similar to the FEM, the domain is subdivided; however, the deformation characteristics are not taken into account, but rather the mesh is adjusted to define the failure mechanism. The normal and shear forces along interfaces are related via the Mohr–Coulomb failure criterion. More recently, Zhang (1999) and Chen et al. (2003) also combined the ideas of the rigid finite element method (RFEM) and limit analysis to determine the minimum factor of safety within the framework of an optimization problem wherein the objective function and constraint equations are derived from energy considerations, together with the Mohr–Coulomb failure criterion.

Comparison of alternative methods of analysis

It has already been mentioned that the predicted factor of safety can be similar for various assumed forms of failure surface. Figure 2 shows the critical failure surfaces for an example presented by Stolle et al. (2004) that deals with a 12.2 m high 2–1 slope supported by a 1.1 m thick layer of similar material (c' = 28.8 kPa and ϕ' = 20.0°), which in turn is supported by a thin 0.4 m weak layer (c' = 0 kPa and ϕ' = 10.0°) that covers the bedrock. The unit weight of both materials is assumed to be 18.8 kN/m^3. Although the shapes of the critical surfaces are quite different, depending on the nature of the analysis, the resulting critical slip surfaces all correspond to a minimum factor of safety (F_s) of approximately 1.36 to 1.37. This may be a consequence of the presence of a weak layer along the bottom of the embankment. Nevertheless, depending on the inherent assumptions of the analysis, it is not unusual in slope stability analysis to find that the mechanism corresponding to the computed minimum factor of safety may not be unique. Given the variability of the properties of geological materials, which contributes to the uncertainty, one should not

Fig. 1. Slip circle and main force components. *T*, mobilized shear force; *N*, normal force; *W*, weight of the slice; *X*, normal interslice force; *Y*, tangential interslice force; *r*, radius of trial circle; *l*, length of chord for slice; α, angle of chord relative to the horizontal.

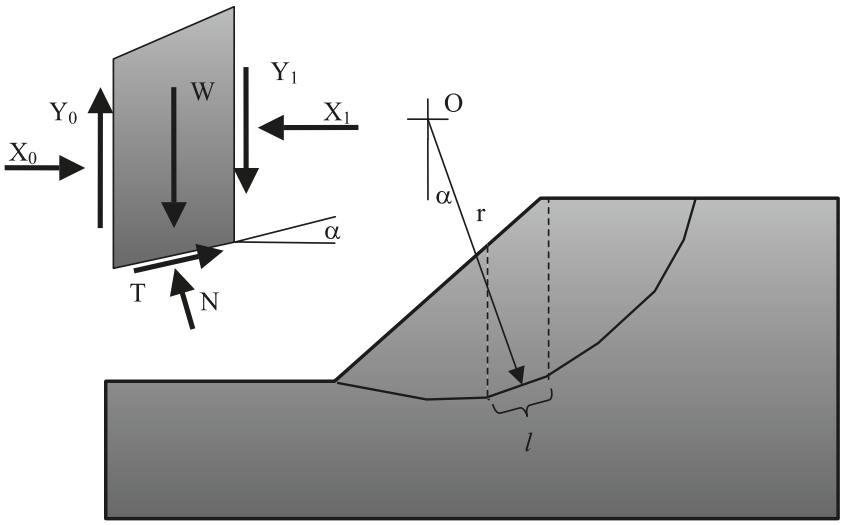

Fig. 2. Critical slip surfaces for slope stability (factor of safety is approximately 1.36–1.37) (Stolle et al. 2004). FEM, finite element method; KEM, kinematic element method.

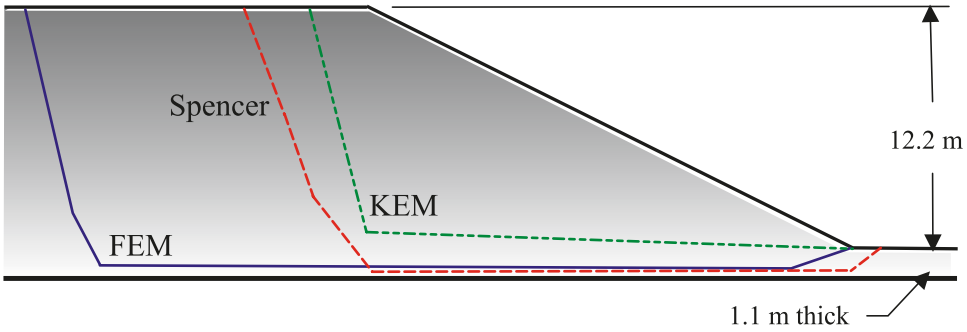

expect that the application of refined models to real world problems can yield more realistic or better solutions. One should therefore ask: how refined should an analysis be in light of the unknowns?

Overview of slip circle analysis

Experience in the past has indicated that computed factors of safety using circular slip surfaces are similar to those from analyses that accommodate more complex surfaces (Chowdhury 1978). Approximations used for the shape of potential failure surfaces are often dictated by convenience rather than the actual geometry of failure. Circular arc analyses, in which the emphasis to check stability is on determining the global factor of safety (F_s) with respect to moment equilibrium, are preferred owing to the simplifications that are encountered in such analyses.

Consider a potential circular failure surface of the slope shown in Fig. 1 and the subdivision of the mass into a number of slices (only one being shown), wherein the forces acting on a slice consist of the weight (*W*), tangential (*Y*) and normal (*X*) interslice forces, as well as the normal (*N*) and mobilized shear (*T*) forces along the bottom of the slice. A rigorous solution requires that both force and moment equilibrium of each slice (local equilibrium) be satisfied, as well as that on the mass as a whole (global equilibrium). To render the statically indeterminate analysis determinate, assumptions between slices are required. Depending on the assumptions regarding the interslice forces *X* and *Y*, various definitions for F_s have been developed. The consequences of modeling assumptions are briefly illustrated for two of the simpler approaches; namely for the Fellenius and modified Bishop's methods.

Taking into account all slices, moment equilibrium about O yields $\Sigma Tr = \Sigma Wr\sin\alpha$, where *r* is the radius of the trial circle, and α is the angle of the chord relative to the horizontal. For each slice we have a situation where, for local equilibrium, the mobilized shear is less than that corresponding to failure T_f and therefore given $T \leq T_f = \tau_f l$ we have $\Sigma W\sin\alpha \leq \Sigma \tau_f l$, in which τ_f is the shear stress that is given by the Coulomb failure criterion $\tau_f = c + \sigma_n\tan\phi$, with ϕ being the friction angle, *c* the cohesion, σ_n the normal force on the surface on which the shear stress acts, and *l* is the length of chord defined in Fig. 1. We can now proceed to define the factor of safety with regard to moment equilibrium,

$$[1] \qquad F_s = \frac{\Sigma \tau_f l}{\Sigma W\sin\alpha} \Rightarrow F_s = \frac{\Sigma (cl + N\tan\phi)}{\Sigma W\sin\alpha}$$

recognizing that the normal force is related to normal stresses via $N = \sigma_n l$. As far as the exposition here is concerned,

no distinction is made between total and effective stress analysis with the understanding that the influence of pore pressure must be considered when dealing with situations where pore pressure is important.

Equation [1] reinforces the fact that the numerator reflects the strength characteristics of the material, the supply, with the denominator capturing the demand attributed to the external loading. It is important to recognize that we have not attempted to satisfy $\Sigma\vec{F} = 0$ on the global and local levels. The difference between the various procedures depends on how force equilibrium is satisfied. For example, by ignoring the interslice forces and considering only force equilibrium at the slice level, one obtains the relation for factor of safety attributable to Fellenius (1936)

$$[2] \qquad N = W\cos\alpha \;\Rightarrow\; F_s = \frac{\Sigma\,[cl + (W\cos\alpha)\tan\phi]}{\Sigma\, W\sin\alpha}$$

Alternatively, by considering the vertical equilibrium of a slice and recognizing that $T \le T_f = \tau_f l$, one arrives at a modified Bishop's relation

$$[3] \qquad N \ge \frac{W - cl\sin\alpha - \Delta Y}{\cos\alpha + \tan\phi\sin\alpha} \;\Rightarrow\; F_s \cong \frac{\Sigma\left[cl + \left(\dfrac{W\tan\phi + cl\cos\alpha}{\cos\alpha + \tan\phi\sin\alpha}\right)\right]}{\Sigma\, W\sin\alpha}$$

after assuming that the influence of the interslice force difference ΔY is small when compared to slice weight W and cohesion c. Strictly speaking, the assumed insensitivity of F_s to interslice shear is only true for circular slip in a homogeneous soil. Equation [3] is slightly different from that usually presented, see, for example, Craig (1997), as a factor of safety term does not appear on the right hand side of the equation. This term was eliminated by adopting the more realistic and accurate assumption $T \le T_f$ that takes into account progressive yielding.

A comparison of eqs. [2] and [3] clearly illustrates that the factor of safety calculation is sensitive to assumptions with respect to interslice forces and equilibrium. As indicated by Craig (1997), the Fellenius procedure usually underestimates the factor of safety by 5% to 20% when compared with more refined analyses, with the Bishop's method usually performing much better. Improvements to F_s estimates are possible by more rigorous approaches taking into account the interslice forces via force equilibrium. Without considering the deformation characteristics of the slope, this can only be accomplished by making assumptions on their distribution along the slope, as shown by Morgenstern and Price (1965). To make the system of equations statically determinate, their method introduces a relation between interslice forces of the form $Y = \lambda f(x)X$, with λ being a scaling factor and function $f(x)$ being chosen to take into account the variation of the ratio of shear to normal force (Y/X) along the slope. A drawback of the procedure is the assumption required regarding the distribution of the ratio Y/X. The following section develops a rigid finite element procedure to overcome this perceived drawback.

Mathematical formulation for force equilibrium

This section describes a mathematical model based on rigid elements and a nonlinear constitutive law that relates interface stresses to displacement discontinuities for determining the forces between slices and at their base along the failure surface. Up to this point, the usual soil mechanics convention of compression positive has been adopted. For the theoretical development in this section, the convention of tension being positive is followed.

Equilibrium

We begin by writing a weak form of force equilibrium of the domain of interest by using an extended form of the principle of virtual work, in which the statically admissible stress distribution satisfies

$$[4] \qquad \int_V \boldsymbol{\delta\varepsilon}^T\boldsymbol{\sigma}\,\mathrm{d}V + \int_{S_i} \delta\Delta\mathbf{u}^T\mathbf{p}\,\mathrm{d}S - \int_{S_T} \boldsymbol{\delta}\mathbf{u}^T\mathbf{t}\,\mathrm{d}S - \int_V \boldsymbol{\delta}\mathbf{u}^T\mathbf{b}\,\mathrm{d}V = 0$$

where $\delta\boldsymbol{\varepsilon}$ is the virtual strain consistent with virtual displacements $\boldsymbol{\delta}\mathbf{u}$, $\mathbf{b}$ are the body forces in domain V, $\mathbf{t}$ are the surface tractions on boundary S_T, and $\boldsymbol{\sigma}$ are the stresses, with the vector $\mathbf{p}$ representing the interface stresses or the stresses at bottom of slices that are related to the relative displacement $\Delta\mathbf{u}$ between two rigid elements or the sliding and stable body. The domain is bounded above by the free surface and surface loading, and below by an assumed failure surface. As with the traditional slope stability algorithms, an objective of the analysis is the identification of the critical surface that minimizes the factor of safety. For purposes of this study the slip surface is assumed to be circular.

Within the context of the FEM and recognizing that the strains within the rigid elements vanish, eq. [4] may be simplified in discretized form as

$$[5] \qquad \int_{S_i} \mathbf{N}^T\mathbf{p}\,dS - \int_{S_T} \mathbf{N}^T\mathbf{t}\,dS - \int_V \mathbf{N}^T\mathbf{b}\,dV = \mathbf{0}$$

where $\mathbf{N}$ refers to the shape functions for the displacement jumps; that is, $\Delta\mathbf{u} = \mathbf{Na}$ with $\mathbf{a}$ containing the vector of element displacements that are to be determined. The integral that contains $\mathbf{p}$ corresponds to interface elements; see, for example, Potts and Zdravkovic (1999). Since the domain elements are rigid, the horizontal and vertical displacements $\mathbf{u} = \langle u \quad v \rangle^T$ within each rigid element are constant.

Constitutive description

To simplify this presentation, the relation between the displacement discontinuities and interface stresses is developed here for the conditions along the failure surface, wherein the relative displacement between a rigid slice and the rigid material along the base is given by $\mathbf{u}$. When considering the constitutive conditions between slices, $\mathbf{u}$ is replaced by $\Delta\mathbf{u}$.

Referring to Fig. 1, let us define a local coordinate system inclined at an angle α with respect to the horizontal such that the vector $\overline{\mathbf{u}} = \langle \overline{u} \quad \overline{v} \rangle^T$ contains the displacement components parallel and perpendicular to the basal surface. Within the local frame of reference, the tangential shear

stress τ_n and the normal σ_n stress are related to the displacement jumps via the relation

$$[6] \qquad \begin{Bmatrix} \tau_n \\ \sigma_n \end{Bmatrix} = \begin{bmatrix} K_t & 0 \\ 0 & K_n \end{bmatrix} \begin{Bmatrix} \overline{u} \\ \overline{v} \end{Bmatrix}$$

in which

$$[7] \qquad K_t = k_t + \frac{\langle F \rangle}{|\overline{u}| + a}$$

with $F = c - \sigma_n \tan\phi$ being the Coulomb yield function such that $\langle F \rangle \geq 0$, k_t is the limiting residual stiffness corresponding to failure conditions, a is a constant that ensures that the denominator is not zero and is selected in such a way that $K_t \gg k_t$ when the stresses are well below yield; that is, $\tau_n - c + \sigma_n \tan\phi \leq 0$. For this study a = 0.000 01, with k_t = 10^3 and 10^2 kPa/m for the failure surface and interslice interfaces, respectively. A lower value of shear stiffness for the interslice forces was selected to ensure that failure conditions occurred first on the slip surface. Scrutiny of eqs. [6] and [7] reveals that at a low shear stress relative to failure, the tangential displacement is small and due to high shear stiffness. As failure is approached the shear displacement becomes large and the shear stiffness approaches its residual value.

A similar function is selected for the normal stiffness, in which

$$[8] \qquad K_n = \begin{cases} K_{no} & v \leq 0 \\ k_{nr} + \dfrac{\kappa}{\overline{v} + A} & v > 0 \end{cases}$$

where K_{no} is the interface stiffness when it is in compression, k_{nr} ($\ll K_{no}$) is the residual stiffness if the surface is in tension, κ is a constant, and $A = \kappa/(K_{no} - k_{nr})$. For this study κ was chosen to be 1 kPa and $k_{nr} = K_{no}/100$, with K_{no} = 10^8 kPa/m. The stiffness coefficients were chosen in such a way as to ensure that the sliding stiffness was less than the normal stiffness, which has to be large in compression to minimize the relative normal displacement of an interface.

Taking into account the usual vector transformations, eq. [6] can be converted to the global frame of reference, in terms of the horizontal (p_x) and vertical (p_y) stress vector components; that is,

$$[9] \qquad \begin{Bmatrix} p_x \\ p_y \end{Bmatrix} = \begin{bmatrix} K_t\cos^2\alpha + K_n\sin^2\alpha & (K_t - K_n)\cos\alpha\sin\alpha \\ (K_t - K_n)\cos\alpha\sin\alpha & K_n\cos^2\alpha + K_t\sin^2\alpha \end{bmatrix} \begin{Bmatrix} u \\ v \end{Bmatrix}$$

or $\mathbf{p}_i = \mathbf{k}_i\mathbf{u}_i$, in which the subscript i refers to the node (element) number. A superscript j, which can take on values (l, r, b) denoting the left, right, and bottom boundaries, respectively, is introduced at this point. By defining ℓ_i to be the length of an interface, the equilibrium equation corresponding to node i is

$$[10] \qquad -\ell_i^l\mathbf{k}_i^l\mathbf{u}_{i-1} + (\ell_i^l\mathbf{k}_i^l + \ell_i^b\mathbf{k}_i^b + \ell_i^r\mathbf{k}_i^r)\mathbf{u}_i - \ell_i^r\mathbf{k}_i^r\mathbf{u}_{i+1} = \begin{Bmatrix} F_x \\ -\gamma V_i + F_y \end{Bmatrix}$$

where F_x and F_y denote surface loading on an element arising from traction $\mathbf{t}$, and the other parameters are the same as defined previously. Close scrutiny of eq. [10] reveals that both local and global equilibrium are being satisfied.

Fig. 3. Location of integration points at which plasticity occurs.

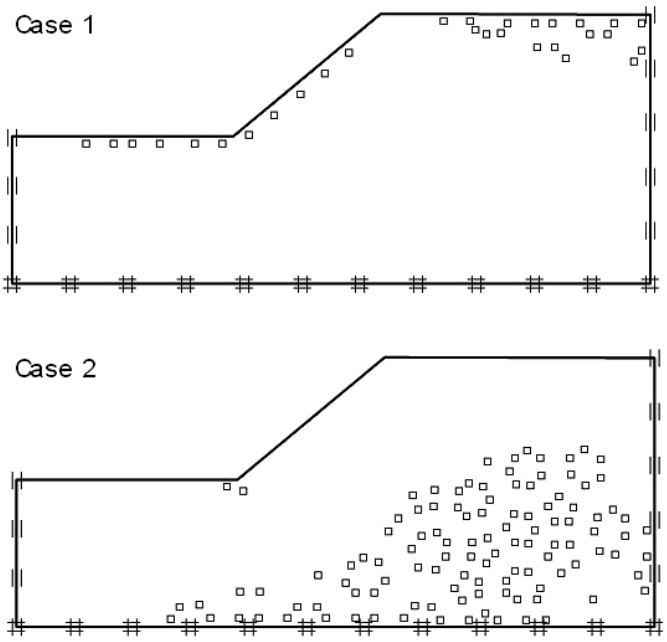

Numerical implementation

As with the traditional limit equilibrium approach, a failure surface must be assumed with the slope subdivided into slices. For the proposed procedure, the interslice forces are determined via a finite element analysis, with the resulting forces used to establish, for example, the factor of safety with respect to moments. Given that the constitutive law is nonlinear, a direct iteration scheme has been adopted where $\mathbf{a}_{n+1} = \mathbf{f}(\mathbf{a}_n)$ with the load remaining constant. Convergence is assumed to be attained when $\eta \geq \sqrt{\Delta\mathbf{a}^T\Delta\mathbf{a}}/\sqrt{\mathbf{a}^T\mathbf{a}}$ where η is the tolerance (~0.001) and $\Delta\mathbf{a}$ implies changes in displacements between two iterations. Given that the half bandwidth (3) of the stiffness matrix is small and that relatively few slices are required for analysis, the computation of the global factor of safety is relatively quick.

Although outside the scope of the current study, it should be noted that the finite element routine must be placed within an optimization algorithm to search for the failure surface that minimizes the factor of safety.

Numerical examples

The objectives of the following example are to investigate the influence of interslice forces on the global factor of safety and the distribution of the local factor of safety along the bottom of each slice, taking into account the relative displacements. While the local factors of safety are known at failure, their distribution is not clear for conditions below failure. Similar analyses have been carried out by others; see, for example, Spencer (1967). In the investigation carried out in this study, the interslice forces are not assumed, a priori, but rather are determined as part of the solution, depending on the relative displacements. The predictions of the proposed model are compared to those obtained via the

Fig. 4. Potential failure mechanisms for cases 1 and 2 (r = 42 m).

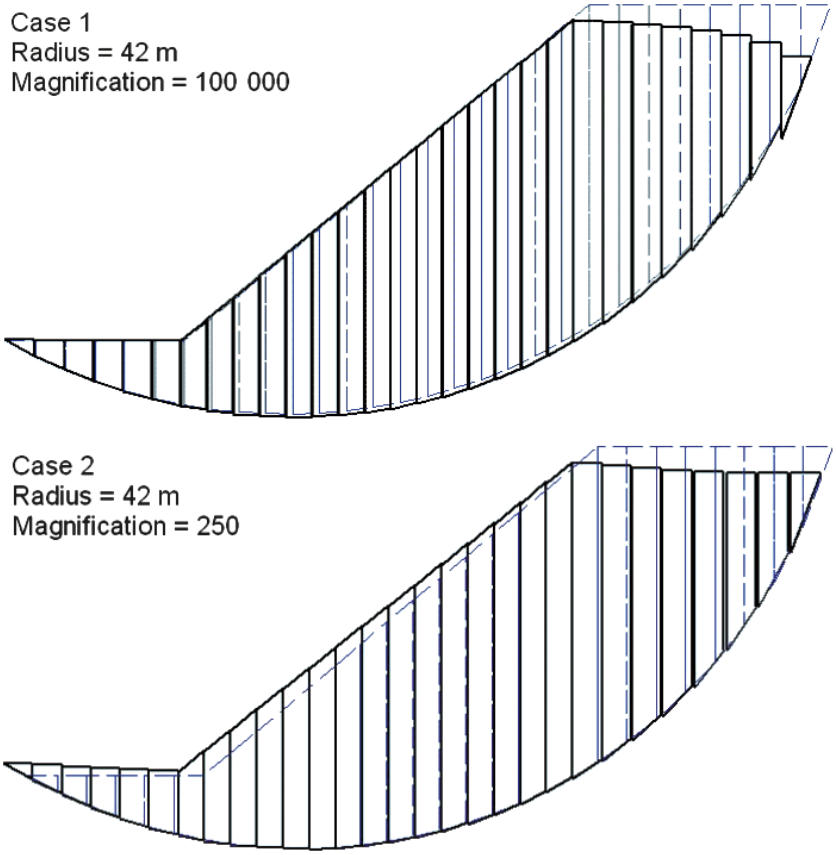

traditional approaches, including the Fellenius, Bishop's and Morgenstern–Price (M–P) methods. Although the M–P simulations were performed using $f(x)$ = constant, it was found that the use of the half sine wave distribution provided similar predictions.

We consider a slope similar to the one shown in Fig. 1, in which the height is 25 m and the slope inclination is $\theta \approx 40^\circ$; that is, $\tan\theta = 5/6$. Four slope stability cases are considered: case 1 — homogeneous cohesionless material with $\phi = 40^\circ$; case 2 — homogeneous cohesive material with c = 50 kPa; case 3 — homogeneous mixed soil with $\phi = 20^\circ$ and c = 30 kPa; and case 4 — homogeneous cohesionless embankment with $\phi = 40^\circ$ supported by a foundation consisting of the material used in case 3. The unit weight of all materials was assumed to be 18.5 kN/m^3. All results reported for this example correspond to slip circles that have coordinates (7.5 m, 36.5 m) for the center of rotation relative to the toe of the circle.

Plasticity and deformation characteristics

Before investigating the stability of the slope for various failure criteria, nonlinear finite element analyses for cases 1 and 2 were completed assuming Mohr–Coulomb failure to obtain a sense of the distribution of yielding as the gravity load is increased; see Fig. 3, which shows integration points where yielding was detected before reaching collapse. As one might expect, the development of plastic zones for cohesionless and cohesive materials are very different, demonstrating the need to take into account, at least in an approximate way, the evolution of yielding. Figure 4 compares the same two cases corresponding to a circular arc of 42 m. The fact that the magnification of the deformed configuration for case 1 is much greater than that for case 2 reflects the fact that the factor of safety (F_s) is much greater. A close examination of the deformed configurations corresponding to the potential failure surfaces reveals differences in the relative displacements and the evolution of yielding. Important observations are: (*i*) that tension develops in the cohesive soil at the top of the circle; and (*ii*) that the entire mass appears to be moving, which is different from case 1, where the movement is primarily at the top of the circle. These observations are consistent with the development of plastic zones for each case shown in Fig. 3. It must, however, be stressed that the slip circle results do not necessarily correspond to the failure surface.

Factor of safety as a function of radius

An analysis of the slope was originally completed using the traditional methods of slices. Thereafter a representative location for the center of rotation for potential slip circles was selected to perform a sensitivity analysis upon, using a slice width of 2 m wide or less. It was found that F_s did not change much with further increases in refinement. From previous analyses it had been observed that the factor of safety tends to increase for a homogeneous embankment constructed of cohesionless soil, but decrease for the case of a cohesive soil, when the number of slices increases. Figure 5 summarizes the factors of safety as a function of the radius of the circle. The results for the cohesive soil (case 2), which are not unexpected, clearly show that the factor of

safety decreases with an increase in radius and is independent of interslice force considerations. However, the value of F_s is relatively insensitive to radius beyond 33 m. This is not surprising considering that a large zone within the embankment is yielding even before collapse takes place. For the cases of cohesionless and mixed soils, one observes that the value F_s is sensitive to the assumptions dealing with the interslice forces. Although Bishop's procedure is often recognized as being more accurate, one observes, at least for case 1, that the global F_s using the Fellenius procedure better approximates those predicted by the RFEM. The opposite is true for the slope consisting of the mixed soil.

Although not shown, the factors of safety predicted by the M–P procedure were almost identical to those of the proposed approach.

Conditions along assumed slip surface

Figure 6 summarizes the results from the finite element analyses for the variation in local factor of safety, shear stress, and normal pressure for the four cases, with the assumed slip surface having a radius of 42 m. The values of the local factor of safety F_{sl} are given by $F_{sl} = \langle F \rangle / (K_t \overline{u})$, which clearly indicates that the local value depends on relative displacement. For this particular slope and assumed form of failure one observes that the values of F_{sl}, which compare shear strength to mobilized shear, don't vary much, particularly when $F_{sl} < 1.6$ (Fig. 6*a*). On the other hand, for higher factors of safety, as is the case for the slope consisting of cohesionless material, the variation in F_{sl} is clearly noticeable. It should be noted that for the form of constitutive relation adopted in this study, the predicted F_{sl} cannot be much less than 1, even though the global F_s is much less, as shown in Fig. 5. This is apparent for case 2, where we have a cohesive soil with the factor of safety and basal shear stress being relatively constant.

The predictions for stresses along the base from the M–P procedure were almost identical to those of the proposed approach. On the other hand, while the proposed procedure predicted some variation in the local factor of safety, the values of F_{sl} predicted by the M–P procedure were constant, having values for cases 1, 3, and 4 of 2.24, 1.61, and 1.38, respectively. These values are approximately the same as those predicted by the proposed approach for the interval 10–30 m. As far as case 2 is concerned, the M–P method had difficulty converging to a solution. With regard to basal stresses, there is a jump in shear stress for the two-layered system (case 4) because of changing material properties as the slip surface moves through one material into the other (Fig. 6*b*). The results indicate that the basal pressure is not very sensitive to material type, as shown in Fig. 6*c*. However, at the top of the slip circle, the cohesive soil undergoes some tension.

Conditions along element interfaces

Figure 7 summarizes the stress conditions at the vertical interfaces along the slope, with Fig. 8 showing the interslice forces obtained using the finite element procedure, as well as the M–P method with $f(x)$ = constant. With regards to the pressures, no special provisions were made, except for reducing stiffness, for the situation where an interface went into tension, which turned out to be primarily for case 2 involving the cohesive material. An examination of Fig. 7 clearly indicates that the interface pressures are sensitive to the material that one encounters. As far as the forces are concerned (shown in Fig. 8) the overall variations in normal force as predicted by the RFEM and M–P simulations are similar. Except for case 2, the mobilized interslice shear stresses are relatively small and uniform, which is responsible for the small forces P_y (also denoted as Y in Fig. 1) shown in Fig. 8, at least for the results corresponding to the RFEM simulations. The differences between the RFEM and M–P predictions may be attributed to the way in which the

Fig. 5. Comparison of factors of safety as a function of radius, cases 1 to 3.

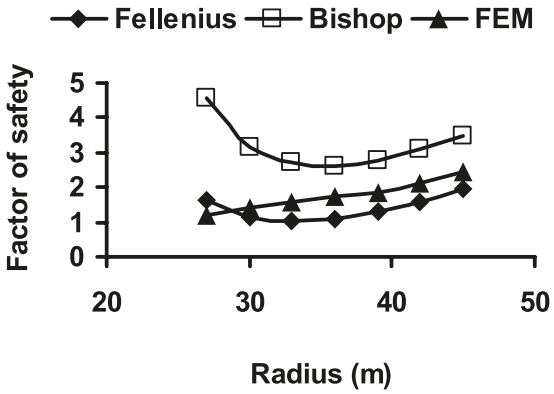

(a) Case 1

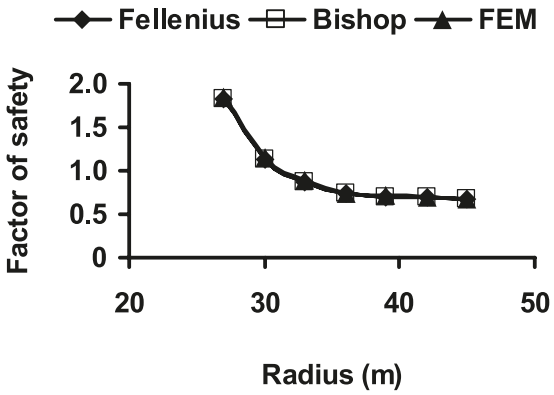

(b) Case 2

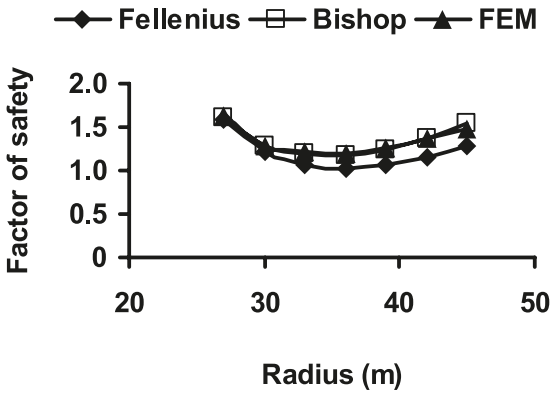

(c) Case 3

Fig. 6. Conditions along the potential slip surface (r = 42 m).

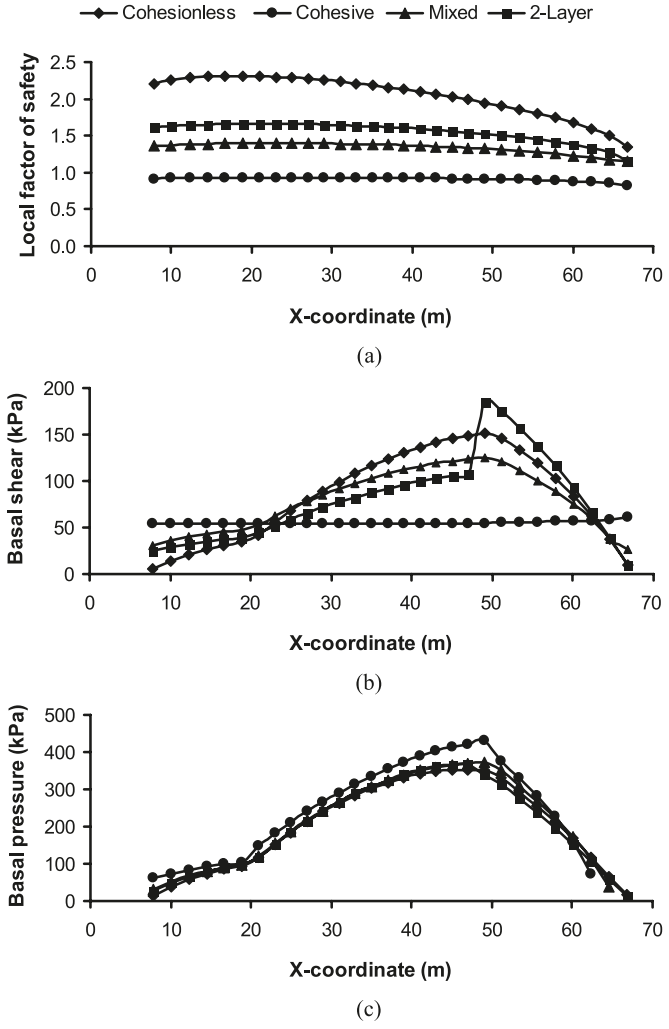

Fig. 7. Conditions between slices corresponding to simulations (r = 42 m). p_x, p_y, horizontal and vertical stress vector components, respectively.

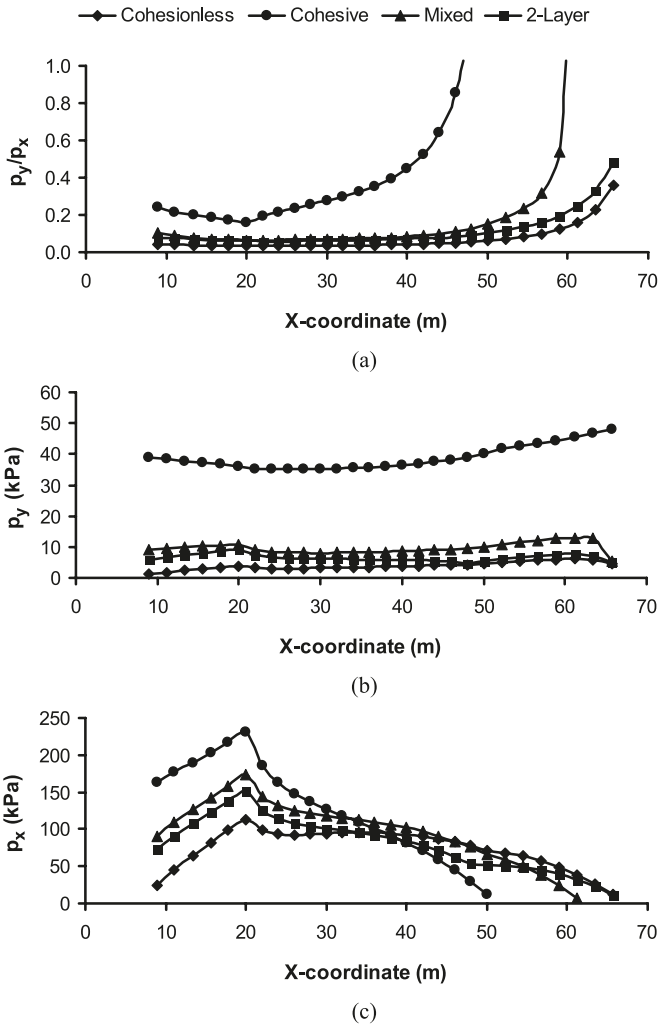

ratio p_y/p_x from the two procedures is handled. For the FEM simulations, it is part of the solution, being related to the deformation characteristics, whereas in the M–P analyses the distribution of this ratio must be specified, a priori. For the analyses of the cohesionless, mixed and two-layer soil slopes, the M–P approach predicted p_y/p_x constants of 0.37, 0.32, and 0.33, respectively. These values are higher than those predicted from the RFEM analyses along most of the slope.

A comparison of the net shear force on a slice relative to its weight confirms that the practice of neglecting the effect of ΔY is reasonable. For the examples presented in this paper, the ratio $\Delta Y/W$ tended to be less than 0.05, and usually much closer to 0.01. This observation is what one might expect for a circular slip mechanism, where one would expect little relative movement between slices. An examination of the ratio p_y/p_x reveals that the ratio is relatively constant, except near the end, mainly because of the small value of the pressure. The higher values of this ratio at the upper end of the sliding surface are reasonable given the large angle of this surface relative to the ground surface at the crest of the slope. It turns out that the analysis, in which the interface pressures are the greatest or vary the most (case 2), showed the least sensitivity with regard to the prediction of the global and local factors of safety. This may be attributed to the failure criterion being independent of pressure and the basal shear stress having attained a limiting value. The large values of the ratio are due to the normal pressures becoming small, even negative and not due to the value of the shear stress.

Influence of surface load

In spite of some differences with regard to the interface forces, the M–P procedure and the proposed method provided similar predictions for conditions along the base. Inherent in the M–P method, however, is the assumption that the factor of safety is constant. This assumption was reasonable for three of the four cases examined.

There are situations where the interslice force details and their influence on the factor of safety may be important, such as for the following example involving a surface load. A natural question that arises is: What is the effect of a surface load on the local factor of safety? To address this query, the proposed model was used to analyze a situation

Fig. 8. Interslice forces along slope corresponding to $r = 42$ m. P_x, P_y, horizontal (X) and vertical (Y) internal force components, respectively.

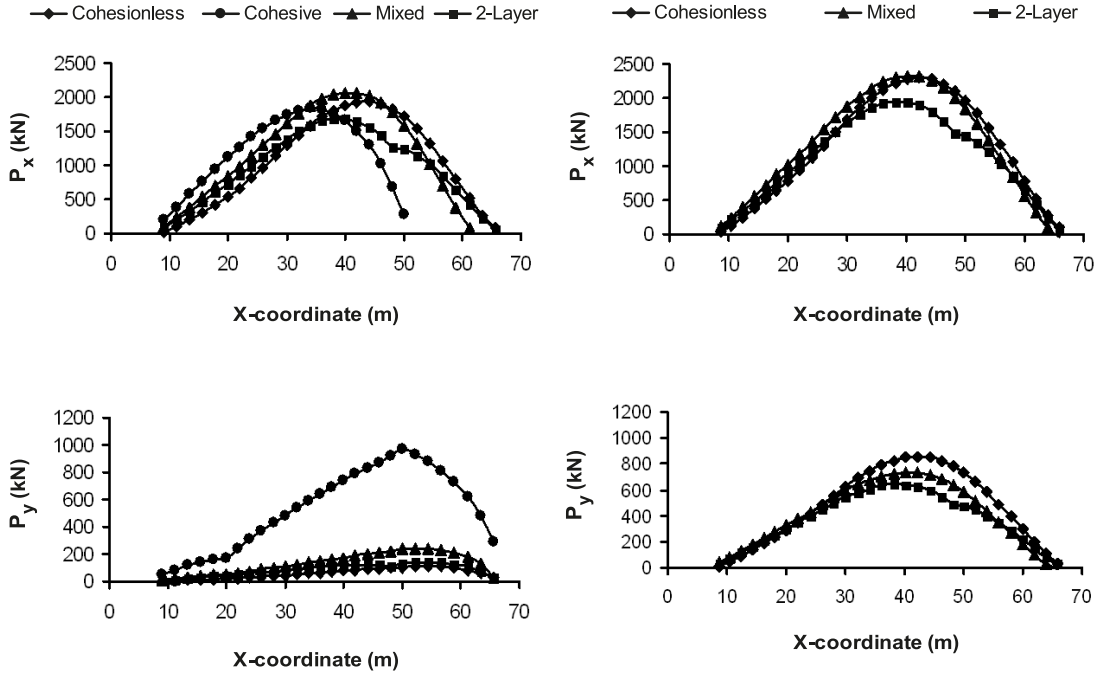

where a 200 kN/m line load was applied to the surface of the slope directly below the center of rotation, assuming the properties of case 3. One observes in Fig. 9 that the load increases the nonuniformity of F_{sl}, as one might expect. For the slip circle analyzed, the surface load has a stabilizing effect due to larger basal pressure. Because of this higher pressure, the local stiffness of the interface is greater and therefore the interface at this location experiences a larger basal shear, which is consistent with what one might expect. As far as the interslice forces are concerned, the influences are small. One should note that the scale for $P_y(Y)$ covers a much smaller range than that for $P_x(X)$.

Concluding remarks

The emphasis in the numerical example has been on investigating the impact of interslice forces on factor of safety calculations for circular failure patterns. While engineering experience and judgement can be introduced into slope stability models to simplify analyses and more specifically to render the system of equations determinate, such a practice could conceivably lead to modeling errors. However, for the slope and form of failure analyzed in this paper, the predictions with regard to the conditions along the slip circle from the Morgenstern–Price analysis were close to those of the proposed method, even though the interslice forces were not the same. Nevertheless, as far as slope stability is concerned, the interslice forces should take into account the progressive nature of failure, which is reflected by the varying local factor of safety. The proposed approach provides additional information on the relative displacements between elements that is not necessarily captured by the traditional approaches.

Fig. 9. Effect of surface load on F_{sl}, basal stresses, and interslice forces ($r = 42$ m).

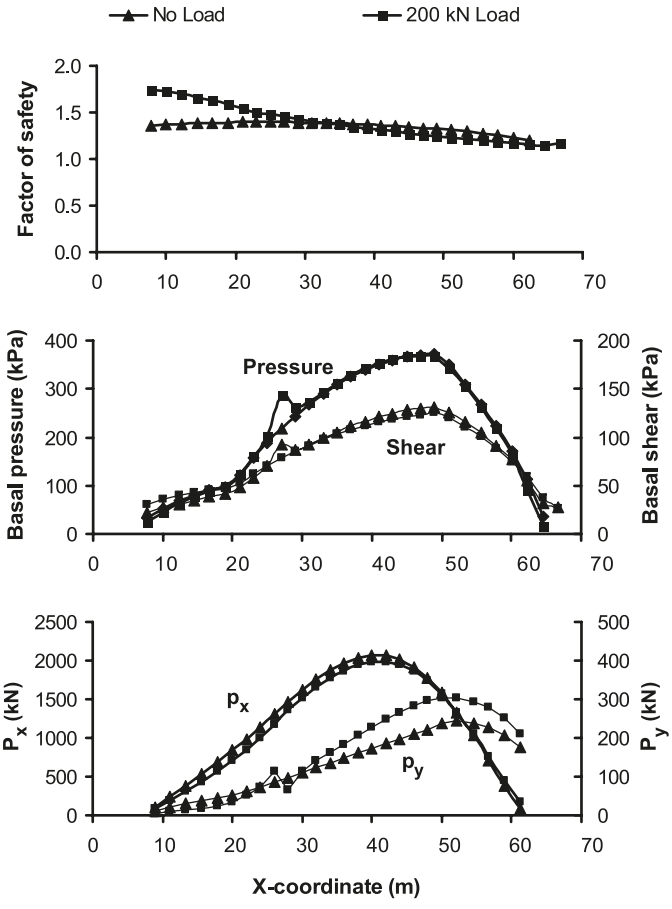

Further research is required on developing strategies for optimum selection of the stiffness characteristics of the interfaces. While a sensitivity analysis had indicated that the results in general were not very sensitive to the exact value of k_t for interslice forces, the range of appropriate values needs closer scrutiny, as do the values for the other stiffness coefficients. An alternative procedure that warrants investigation would be replacing the rigid elements with deformable slices, similar to the procedure presented by Stolle (1988) for the solution of ice creep. Although only circular failure surfaces were considered, the approach presented in this paper can easily be extended to accommodate noncircular failure scenarios, given that the finite element equations satisfy force equilibrium on both the local and global level.

Acknowledgements

The authors would like to thank the Natural Sciences and Engineering Research Council of Canada for its support of this project.

References

Baker, R. 1980. Determination of the critical slip surface in slope stability computations. International Journal for Numerical and Analytical Methods in Geomechanics, **4**(4): 333–359. doi:10.1002/nag.1610040405.

Bishop, A.W. 1955. The use of slip circle in the stability analysis of slopes. Géotechnique, **5**: 7–17.

Chowdhury, R.N. 1978. Slope analysis–developments in geotechnical engineering. Elsevier Scientific Publishing Company, New York.

Chen, Z., and Morgenstern, N.R. 1983. Extension to the generalized method of slices for stability analysis. Canadian Geotechnical Journal, **20**(1): 104–119. doi:10.1139/t83-010.

Chen, Z., and Shao, C. 1988. Evaluation of minimum factor of safety in slope stability analysis. Canadian Geotechnical Journal, **25**(4): 735–748. doi:10.1139/t88-084.

Chen, J., Yin, J.-H., and Lee, C.F. 2003. Upper bound limit analysis of slope stability using rigid finite elements and nonlinear programming. Canadian Geotechnical Journal, **40**(4): 742–752. doi:10.1139/t03-032.

Craig, R.F. 1997. Soil mechanics. 6th ed. E & FN Spon, UK.

De Natale, J.S. 1991. Rapid identification of critical slip surface structure. Journal of Geotechnical Engineering, **117**(10): 1568–1589. doi:10.1061/(ASCE)0733-9410(1991)117:10(1568).

Duncan, J.M., and Wright, S.G. 2005. Soil strength and slope stability. John Wiley & Sons Inc. N.J.

Fellenius, W. 1936. Calculation of the stability of earth dams. *In* Transactions of the 2nd Congress on Large Dams, Washington, D.C., Vol. 4, pp. 445–463.

Fredlund, D.G., and Krahn, J. 1977. Comparison of slope stability methods of analysis. Canadian Geotechnical Journal, **14**(3): 429–439. doi:10.1139/t77-045.

Gussmann, P. 2000. Effective KEM solutions for the limit load and slope stability problem. International Journal for Numerical and Analytical Methods in Geomechanics, **24**: 1061–1077. doi:10.1002/1096-9853(20001210)24:14<1061::AID-NAG111>3.0.CO;2-8.

Kim, J., Salgado, R., and Lee, J. 2002. Stability of complex slopes using limit analysis. Journal of Geotechnical and Geoenvironmental Engineering, **128**: 546–557. doi:10.1061/(ASCE)1090-0241(2002)128:7(546).

Lane, P.A., and Griffiths, D.V. 1997. Finite element slope stability analysis – why are engineers still drawing circles? Numerical Models in Geomechanics - NUMOG VI. *Edited by* S. Pietruszczak and G.N. Pande. A.A. Balkema, London. pp. 589–593.

Li, S.K., and White, W. 1987. Rapid evaluation of the critical slip surface in slope stability problems. International Journal for Numerical and Analytical Methods in Geomechanics, **11**(5): 449–473. doi:10.1002/nag.1610110503.

Malkawi, H., Hassen, W.F., and Sarma, S.K. 2001. A global search method for locating general slip surface using monte carlo techniques. Journal of Geotechnical and Geoenvironmental Engineering, **127**(8): 688–698. doi:10.1061/(ASCE)1090-0241(2001)127:8(688).

Morgenstern, N.R., and Price, V.E. 1965. The analysis of the stability of general slip surface. Géotechnique, **15**(4): 289–290.

Pham, H.T.V., and Fredlund, D.G. 2003. The application of dynamic programming to slope stability analysis. Canadian Geotechnical Journal, **40**(4): 830–847. doi:10.1139/t03-033.

Potts, D.M., and Zdravkovic, L. 1999. Finite element analysis in geotechnical engineering. Thomas Telford, London.

Sloan, S.W. 1988. Lower bound limit analysis using finite elements and linear programming. International Journal for Numerical and Analytical Methods in Geomechanics, **12**: 61–67. doi:10.1002/nag.1610120105.

Sloan, S.W. 1989. Upper bound limit analysis using finite elements and linear programming. International Journal for Numerical and Analytical Methods in Geomechanics, **13**: 263–282. doi:10.1002/nag.1610130304.

Spencer, E. 1967. A method of analysis of the stability of embankments assuming parallel inter-slice forces. Géotechnique, **17**(1): 11–26.

Stolle, D.F.E. 1988. A one-dimensional model for ice slope creep. Journal of Glaciology, **34**: 1–6.

Stolle, D., Guo, P., Ng, K., and Sedran, G. 2004. Finite element analysis of slope stability. Numerical Models in Geomechanics NUMOG IX. *Edited by* S. Pietruszczak and G.N. Pande. A.A. Balkema, London. pp. 623–630.

Yu, H.S., Salgado, R., Sloan, S.W., and Kim, J.M. 1998. Limit analysis versus limit equilibrium for slope stability. Journal of Geotechnical and Geoenvironmental Engineering, **124**(1): 1–11. doi:10.1061/(ASCE)1090-0241(1998)124:1(1).

Zhang, X. 1999. Slope stability analysis based on the rigid finite element. Géotechnique, **49**(5): 585–593.

Zhu, D.Y., Lee, C.F., Qian, Q.H., and Chen, G.R. 2005. A concise algorithm for computing the factor of safety using the Morgenstern–Price method. Canadian Geotechnical Journal, **42**(1): 272–278. doi:10.1139/t04-072.

Zolfaghari, A.R., Heath, A.C., and McCombie, P.F. 2005. Simple genetic algorithm search for critical non-circular failure surface in slope stability analysis. Computers and Geotechnics, **32**(3): 139–152. doi:10.1016/j.compgeo.2005.02.001.